NANO LETTERS

pubs.acs.org/NanoLett

Domain Bundle Boundaries in Single Crystal $BaTiO_3$ Lamellae: Searching for Naturally Forming Dipole Flux-Closure/Quadrupole Chains

L. J. McGilly, A. Schilling, and J. M. Gregg*

Centre for Nanostructured Media, School of Maths and Physics, Queen's University Belfast, University Road, Belfast, BT7 1NN. U. K.

ABSTRACT Naturally occurring boundaries between bundles of 90° stripe domains, which form in $BaTiO_3$ lamellae on cooling through the Curie Temperature, have been characterized using both piezoresponse force microscopy (PFM) and scanning transmission electron microscopy (STEM). Detailed interpretation of the dipole configurations present at these boundaries (using data taken from PFM) shows that in the vast majority of cases they are composed of simple zigzag 180° domain walls. Topological information from STEM shows that occasionally domain bundle boundaries can support chains of dipole flux closure and quadrupole nanostructures, but these kinds of boundaries are comparatively rare; when such chains do exist, it is notable that singularities at the cores of the dipole structures are avoided. The symmetry of the boundary shows that diads and centers of inversion exist at positions where core singularities should have been expected.

KEYWORDS Ferroelectric domains, vortices, quadrupole, flux closure, piezoresponse force microscopy

In 1946, Kittel proposed that magnetic domains in small-scale crystals should form into quadrant blocks, separated by 90° domain walls, since in this geometry energetically favorable flux-closure could be realized.[1] Subsequent experimental domain studies have shown these kinds of quadrant structures to be commonplace.[2−5] Nevertheless, the relatively recent discovery of the magnetic vortex,[6] a derivative of the original Kittel pattern, in which flux-closure is achieved through spatially continuous rotation of magnetization, has created a great deal of renewed excitement among the scientific community. Eager studies into the properties of this "ferrotoroidal" state have abounded.[7−11]

Given the similarities between ferromagnetism and ferroelectricity, the possibility that analogous ferroelectric vortices might also exist has been tantalising. Yet, despite the encouragement given by the ground-breaking atomistic simulations performed by Bellaiche and co-workers[12−16] in which ferroelectric vortices have been predicted in extremely small nanostructures, experimental evidence for their existence has been tenuous; Gruverman et al.[17] indirectly inferred the transient existence of a dipole vortex in disk-shaped thin film capacitors. They mapped the development of the out-of-plane polarization during switching and found that it matched predictions from modified Landau−Lifshitz−Gilbert (LLG) finite element models. In-plane behavior could not be measured but was assumed to also be accurately represented by the LLG modeling, which showed that a transient in-plane vortex helped to mediate switching. While reasonable, this inference ignored the possibility of a switching mechanism in which simple 180° domains nucleate and grow around the capacitor perimeter[18] without any mediating in-plane vorticity. Given the high tetragonality and polar anisotropy associated with the composition of ferroelectric investigated ($PbZr_{0.2}Ti_{0.8}O_3$) this less exotic switching mechanism should certainly be considered as a possible alternative to the vortex model proposed. In a separate study, Rodriguez et al.[19] inferred dipole vortices through the nature of the in- and out-of-plane piezoresponse force microscopy contrast seen on PZT nanodots (made by deposition through a nanoporous alumina template). Conclusions were based on matching observations to the modeled contrast expected from a vortex. However, contrast commensurate with a dipole vortex was only seen in a few of the large array of nanodots imaged; in addition, alternative domain patterns that may have produced similar contrast were not extensively considered.

Vortex structures aside, it is remarkable that even the simple flux-closure quadrants envisioned by Kittel have been difficult to find in ferroelectrics. Schilling et al.[20] have seen that clear quadrant structures can form in $BaTiO_3$ nanodots, on cooling through the Curie Temperature but with the complication that each quadrant is composed of a number of 90° stripe domains. In fact, although quadrants might be suggestive of flux-closure, vectorial summing of the inferred local dipole directions within each quadrant generates a broad-brush polar structure that is a quadrupole, and not a

* To whom correspondence should be addressed. Email: m.gregg@qub.ac.uk.
Received for review: 07/22/2010
Published on Web: 09/24/2010

© 2010 American Chemical Society

DOI: 10.1021/nl102566y | *Nano Lett.* **2010,** *10,* 4200–4205

flux-closure state. Some evidence for genuine dipole flux-closure patterns has been presented by Ivry et al.,[21] but the most pertinent observations to date have been made by Balke et al.[22] In their work, dipole patterns at boundaries between packets of domains in $BiFeO_3$, manipulated using a scanning piezoresponse force microscopy (PFM) tip, were investigated. Although dipole vectors were inclined to the $(001)_{pseudocubic}$ surface of the sample (rhombohedral dipole directions in $BiFeO_3$ lie along $\langle 111 \rangle_{pseudocubic}$ directions), the authors pointed out that for some specific boundaries between domain packets the in-plane dipole components formed closure patterns. The resolution of the PFM did not allow these authors to characterize the core of the closure structures in detail, although it could be inferred from their images to sit at the junction between two sets of 90° domain walls.

In this manuscript, we investigate similar, spontaneously occurring, boundaries between parallel sets of 90° domain bundles in thin single crystal lamellae of $BaTiO_3$; only boundaries between domains with fully in-plane polarization have been considered; in this case, in contrast to the studies on rhombohedral $BiFeO_3$,[22] simple flux closure structures without any out-of-plane components are able to form. However, we find that in the majority of cases boundaries between bundles of 90° domains are composed of less exotic zigzag patterns of 180° domain walls. Only rarely do chains of flux-closure and quadrupole structures form, and when they are present we note that domain walls arrange themselves such that core singularities, expected at the center of the flux closure structures, are avoided.

Commercially available polished single crystal $BaTiO_3$ was used as the bulk source material from which $(100)_{pseudocubic}$-oriented thin (~200 nm) lamellar sheets were cut. A FEI200TEM focused ion beam microscope was used for the lamellar machining with processing steps illustrated schematically in Figure 1. A sharp glass needle, controlled with a micromanipulator, was used to remove lamellae from the bulk single crystal; these lamellae were then placed onto MgO single crystal carriers that had been sputter-coated with a platinum thin film (100 nm thick). This platinum acted as a lower electrode for subsequent PFM investigations. Samples were thermally annealed at 700 °C for 1 h in air to fully recrystallize ion-beam-induced surface damage. Annealing also expelled implanted Ga to form gallium oxide islands (Figure 1e) as had previously been observed.[23] A postanneal etch at room temperature in 3 M HCl solution for several minutes was found to be sufficient to remove these gallium oxide islands and leave a smooth undamaged $BaTiO_3$ surface, suitable for PFM measurement (see Figure 1f). To allow an opportunity for equilibrium domain configurations to form, the samples were heated above the Curie temperature (~400 K) and then cooled to room temperature. A Veeco Dimension 3100 with a Nanoscope IIIa controller and EG&G 7265 lock-in-amplifier was used for PFM measurements; a typical probing signal of 3 V_{rms} at a frequency of 20 kHz was

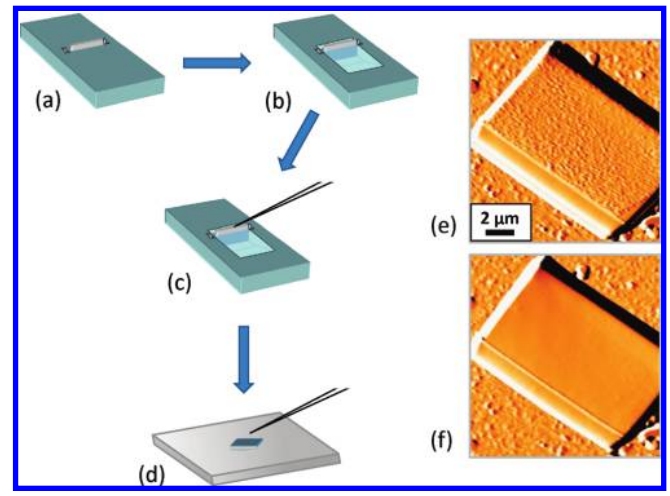

FIGURE 1. Schematic showing protective platinum bar deposition (using focused ion beam-induced local chemical vapor deposition) and machining of a thin lamella (~200 nm thick) from bulk single crystal $BaTiO_3$ (a) and (b). The thin lamella was transferred using a glass needle and micromanipulators (c) onto a platinum-coated single crystal MgO carrier substrate (d). AFM images before (e) and after (f) HCl cleaning etch show how the gallium oxide islands that form after thermal annealing can be effectively removed (note an rms surface roughness of approximately 5 nm in (e) compared to approximately 5 Å measured in (f)).

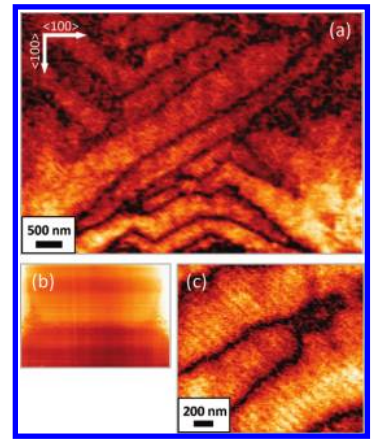

FIGURE 2. Low-magnification PFM amplitude image (a) showing bundles of 90° stripe domains and the dark boundaries between domain bundles. Topography image (b) corresponding to the scan area in (a). Higher-magnification PFM amplitude scan showing enlarged area in which several packets of 90° stripe domains are separated by bundle boundaries (b).

applied to Nanosensors PPP-EFM cantilevers with a force constant of approximately 2.8 Nm^{-1}. For transmission electron microscopy (TEM) investigation, lamellae where lifted out onto 3 mm mesoporous carbon-coated copper grids for analysis with a Tecnai F20 TEM.

Figure 2 shows a number of PFM images from a $BaTiO_3$ lamella prepared in the manner described above. Distinct bundles of stripe domains, present in regular bands, were abundant. These bundles were separated by boundaries predominantly oriented at high angles to the 90° domain walls; by their very nature, these boundaries implied that the configurations of 90° domains differed in detail on either

© 2010 American Chemical Society

DOI: 10.1021/nl102566y | *Nano Lett.* **2010,** *10,* 4200–4205

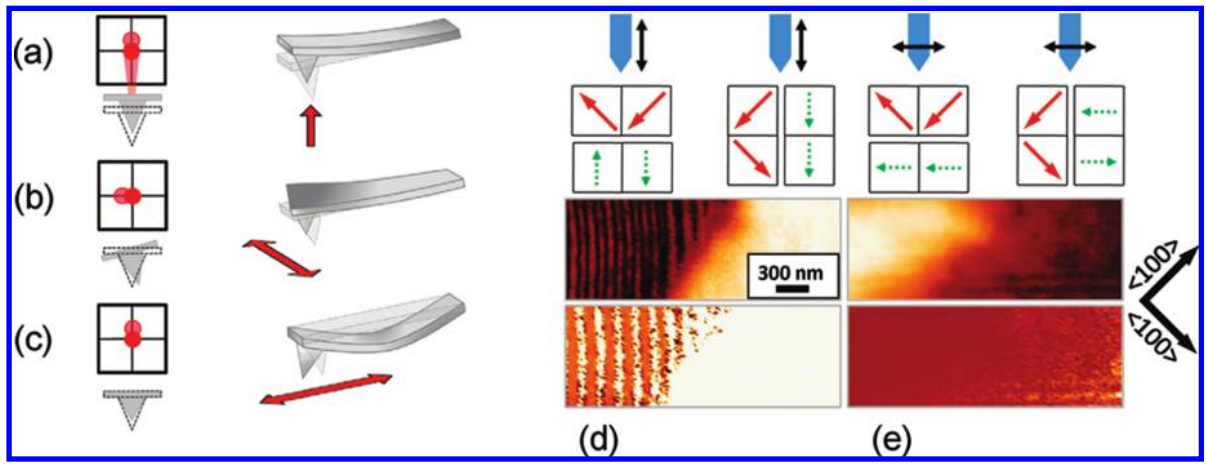

FIGURE 3. Schematic diagrams showing the different cantilever movements associated with the three orthogonal components of electromechanical distortion that are possible in PFM (red double-headed arrows) and the associated deflection of the laser on the microscope photodiode after reflection off the top of the cantilever (a−c). Notice how in-plane electromechanical distortion components, parallel to the axis of the cantilever, result in a longitudinal flexure or "buckling" (c) which causes a vertical deflection of the laser, indistinguishable from the case illustrated in (a). On the right-hand side (d,e) two bundles of domains in a $BaTiO_3$ lamella can be seen from PFM images (amplitude images are above phase images). Domain wall orientations suggest that 90° stripe domains contain polarization directions that are entirely in-plane, thus the vertical electromechanical distortion illustrated in (a) can be ignored, such that all of the vertical movement of the laser spot on the photodiode can be attributed to cantilever flexure. Schematic diagrams illustrate how the flexure mode VPFM and conventional torsional LPFM signals can be used to explicitly map the local domain orientations on either side of a bundle boundary. The cantilever orientation is shown by the solid blue pointer, polar vectors are in red, components of polarization detected are given by the black double-headed arrows next to the cantilevers, and the measured polar components in each case are shown by the dotted green arrows.

side of the boundary, and this was a focus in the current investigation. More detailed analysis of the bundle boundaries required higher resolution PFM data than that shown in Figure 2, and for this an unconventional mode of PFM imaging was used that requires some discussion.

It is generally accepted within the literature that PFM can determine out-of-plane and in-plane domain polarization orientations through discrimination of laser beam deflections that indicate the movement of the cantilever;[24] under the influence of the applied field emanating from the PFM probe tip, an out-of-plane polarization component will produce a piezoelectric electromechanical vertical deformation of the sample surface, which will in turn force a vertical motion of the cantilever. This leads to a measured vertical deflection of the laser beam on the microscope photodetector, as is shown schematically in Figure 3a. Imaging with this information is called "vertical PFM" or VPFM. Correspondingly, an in-plane polarization component can give rise to a torsional distortion of the cantilever that is measured as a lateral deflection of the laser on the photodetector, Figure 3b. Imaging in this mode is known as "lateral PFM", or LPFM. However, the situation can be more complicated. When an in-plane component of the polarization vector lies parallel to the cantilever axis, the resulting in-plane electromechanical deformation can contort the cantilever with neither a vertical movement nor a lateral torsion, but rather with a longitudinal flexure, Figure 3c. This flexure or "buckling" produces a vertical displacement of the laser on the photodetector that is indistinguishable from that associated with genuine vertical cantilever motion. An incorrect assignment of longitudinal tip flexure to indicate vertical electromechanical displacement could easily result, yielding a mistaken apparent vertical polarization component. Longitudinal flexure has already been shown to dominate the piezoresponse signal in certain circumstances and therefore cannot be ignored.[25,26]

In the absence of out-of-plane polarization components, the measured VPFM can entirely and unequivocally be attributed to an in-plane cantilever flexure. In this case, full reconstruction of the in-plane polarization vector can be done by using the VPFM signal to indicate the components of local polarization parallel to the cantilever axis, and LPFM to map the components perpendicular to the cantilever axis. This is precisely the case in the present study: high resolution PFM measurements on the $(100)_{pseudocubic}$ oriented single crystal $BaTiO_3$ lamellar surfaces (Figure 3d,e) revealed fine regular domains of width approximately 80 nm with the vector of intersection between 90° domain walls and the lamellar surfaces orientated along $\langle 110 \rangle_{pseudocubic}$ directions. This contrast, taken together with similar prior images using transmission electron microscopy,[27] implies a microstructure that is entirely composed of in-plane "aa" domains. Thus the VPFM signal obtained (Figure 3d) must be imaging through the longitudinal flexure mode discussed above. As further evidence of this, on rotation of the sample by 90° the observed VPFM domain contrast corresponded exactly to that observed by LPFM when at 0° rotation; the same component of the polarization vector was measured by both modes and showed identical domain contrast. This fact, combined with the precisely known crystallographic orientation of the $BaTiO_3$ lamellae allowed the VPFM signal to be confidently assigned to in-plane flexure behavior. Conse-

© 2010 American Chemical Society

DOI: 10.1021/nl102566y | *Nano Lett.* **2010,** *10,* 4200–4205

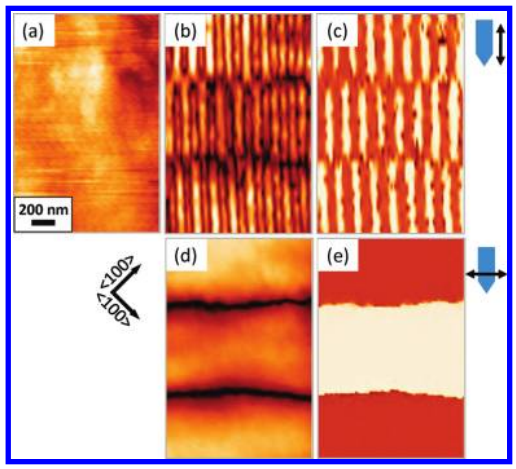

FIGURE 4. High-resolution PFM images of bundle boundaries between three sets of 90° stripe domains. Topography is shown in (a) where the height scale is 2.5 nm; flexural VPFM amplitude is shown in (b) with phase information in (c); torsional LPFM amplitude (d) and phase (e) are shown from the same region. The cantilever diagrams show the in-plane components of polarization detected through each imaging mode.

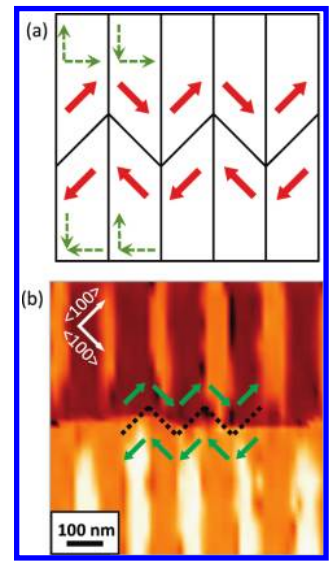

FIGURE 5. Schematic (a) showing the resolved polarization vectors as determined from information garnered from Figure 4. As a 180° change in direction occurs for every polarization vector as it crosses the band boundary, the boundary structure must contain a series of 180° domain walls. Ideally these should be arranged into a zigzag pattern. Combined phase data associated with the band boundary region (b) fails to resolve such a zigzag topology.

quently, two orthogonal in-plane components of polarization were measurable simultaneously in these $BaTiO_3$ lamellae (see the schematics in Figure 3d,e), allowing the local in-plane polarization vector to be fully reconstructed.

In Figure 4, a set of high-resolution PFM images across a typical domain bundle boundary is presented. The sample has been oriented such that 90° domain walls are parallel to the cantilever and are strongly imaged using the flexure VPFM signal, while the bundle boundary is approximately perpendicular to the cantilever, and is strongly imaged in the LPFM signal. To reconstruct the local dipole orientations, the phase information in Figure 4c,e is particularly useful. From Figure 4c, it is clear that the in-plane polarization component, parallel to the cantilever, reverses its orientation across both the 90° domain walls and the domain bundle boundary; by contrast, from Figure 4e, it is clear that the in-plane component of polarization perpendicular to the cantilever remains constant across the 90° domain walls, and only reverses across the bundle boundary. Vectorial summation of the implied components of polarization (both parallel and perpendicular to the cantilever axis within each domain) yields the schematic representation of dipole directions given in Figure 5. Evidently, the bundle boundary is likely to be composed of a series of 180° domains walls arranged in a zigzag fashion. The combined phase information from flexural (VPFM) and torsional (LPFM) imaging modes in Figure 5 shows that the measured topology of the band boundary does not exactly match that predicted insofar as the regular zigzag pattern expected was not strongly observed. Perhaps this is simply a PFM tip resolution issue; however, we also found that bundle boundaries were relatively mobile under imaging fields, and this could also account for some loss of resolution, or smearing of the expected zigzag topology.

Obviously, this type of bundle boundary does not contain the kind of flux closure states previously found in bundle boundaries written into $BiFeO_3$ films by Balke et al.[22] In fact, in all of the PFM investigations that we performed across a number of bundle boundaries in the $BaTiO_3$ lamellae not a single flux-closure system was observed. Presumably, this indicates that in $BaTiO_3$ the zigzag bundle boundary composed of local 180° domain walls is energetically more favorable than that containing a series of adjacent flux closure states. Perhaps the elastic energy due to local disclination strains, required in flux closure loops,[20,28] is part of the story.

In fact, this expectation of elastic disclination strain prompted the use of TEM in the further search for flux closure loops at domain bundle boundaries. Under the TEM, 180° domain walls produce negligible contrast and are difficult to successfully image, whereas the change in unit cell orientation across 90° domain walls renders them readily observable. TEM imaging could therefore be used advantageously to effectively filter out image information from the kinds of 180° bundle boundaries, ubiquitously seen in the PFM investigations described above, and only leave images of bundle boundaries across which domains are reoriented by 90°, along which chains of flux closure loops might be expected.

Figure 6 shows a scanning TEM (STEM) image, using a high angle annular dark field (HAADF) detector, of such a boundary, separating two aa domain bundles. Here, the needlelike point shapes of the 90° domains at the bundle boundary are well resolved, allowing an investigation with greater spatial resolution than would have been possible

© 2010 American Chemical Society

DOI: 10.1021/nl102566y | *Nano Lett.* **2010,** *10,* 4200–4205

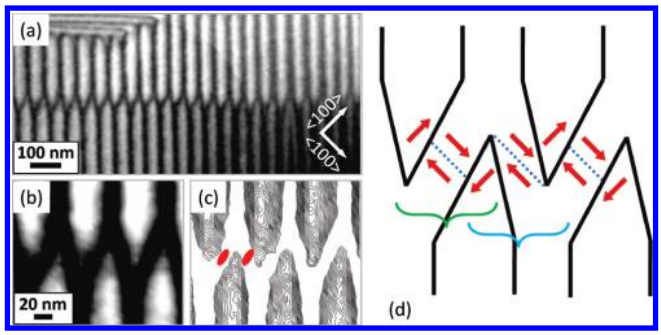

FIGURE 6. STEM images showing two parallel sets of 90° domain bundles and a bundle boundary (a), an enlargement to allow asymmetries in the needle morphology to be clearly seen (b), along with a contour plot of the image intensities (c). The symmetry present in this bundle boundary (lines of diads and centers of symmetry) implies local polarization components such as that proposed in the schematic given in (d). Diad rotational symmetry axes are shown in (c) as red ovals. Inferred 180° domain walls are depicted as blue dashed lines in (d). The flux closure state is highlighted by the green bracket and quadrupole by the blue bracket in (d).

on PFM. Several striking observations can be made. First, the needle point topologies are strongly asymmetric such that the domain wall orientations do not conform strictly to the conventional crystallography of 90° domain walls in a tetragonal material, that is, they do not lie parallel to $\{110\}_{\text{pseudocubic}}$ planes; rather the needles form into asymmetric tapered points. Second, as shown by the image contour plots in Figure 6c, the gradient of the image intensity variation is much greater on one side of the tapered domains than on the other. Moreover, on the upper side of the bundle boundary the steeper gradient in image intensity lies on the left-hand edge of the white stripe domains, while on the lower side it is on the right-hand edge. Both these observations demand the existence of a line of diad symmetry elements (with axes perpendicular to the plane of observation), as well as centers of inversion within the core regions of the bundle boundary. Through Neumann's Principle, the orientations of the dipoles on either side of the bundle boundary must also adhere to this symmetry. To allow this, the only consistent manner in which domain polarization vectors can be arranged is shown schematically in Figure 6d; adjacent flux closure and quadrupole states interlink to form a continuous chain. Quadrupole states exist in unison with closure states and may act to mediate strain and electrostatic interactions between adjacent flux closure loops. Their presence, as inseparable elements of this bundle boundary/flux closure arrangement, changes the feature periodicity from ~30 nm for individual flux closure elements to ~60 nm for closure/quadrupole pairs. Note that unobserved 180° domain walls that pass through both the diads and centers of symmetry are implicit in the schematic representation (but remain undetected by TEM).

It is particularly interesting that in the formation of this boundary simple quadrant flux closure states, where four 90° domain walls intersect at a single point, are avoided. Instead, the flux closure object is "elongated" by the insertion of the 180° domain wall, spatially separating elements of the closure quadrants and avoiding a distinct closure core singularity. The position at which such a singularity would have occurred is instead only marked by the elements of symmetry associated with the boundary. Some insight into this phenomenon may be gained by consideration of work by Srolovitz and Scott;[29] they used two models for assessing the energetic stability of specific domain wall junctions or vertices. A simple Potts' model, where any degree of dipole misalignment between nearest neighbors was not energetically favorable, suggested that 4-fold vertices (where four domain walls meet at a point, as would be the case in a classic quadrant closure domain set) were unstable with respect to the formation of two 3-fold vertices. By allowing some degree of dipole misalignment, through a "vector-Potts'" or clock-model was found to stabilize 4-fold vertices. The avoidance of such distinct quadrant cores in the $BaTiO_3$ bundle boundary junctions observed might therefore reflect an intolerance of dipole misalignments and the importance of the significant anisotropy energy in the system.

In conclusion, boundaries between bundles of 90° domains have been investigated as possible sites for the existence of naturally occurring flux closure states in thin single crystal $BaTiO_3$ lamellae. Detailed examination by PFM showed that abundant bundle boundaries occurred between large scale regions of parallel 90° stripe domains; however, rather than containing flux closure states, these boundaries were found to consist of a series of 180° domain walls arranged ideally into zigzag patterns. Using TEM, occasional band boundaries were found in which, through symmetry arguments, chains of interlinking flux closure and quadrupole states could be inferred. The detailed structure of these boundaries suggested that flux-closure core singularities are avoided in $BaTiO_3$.

Acknowledgment. The authors acknowledge financial support from the Engineering and Physical Sciences Research Council (EPSRC) through Grant Awards EP/F004869/1 and EP/H00307X/1 and the Department for Employment and Learning (DEL).

REFERENCES AND NOTES

(1) Kittel, C. Theory of the Structure of Ferromagnetic Domains in Films and Small Particles. *Phys. Rev.* **1946**, *70*, 965.
(2) Kittel, C. Physical theory of ferromagnetic domains. *Rev. Mod. Phys.* **1949**, *21*, 541.
(3) Özdemir, Ö.; Xu, S.; Dunlop, D. J. Closure domains in magnetite. *J. Geophys. Res.* **1995**, *100*, 2193.
(4) Runge, K.; Nozaki, Y.; Otani, Y.; Miyajima, H.; Pannetier, B.; Matsuda, T.; Tonomura, A. High-resolution observation of magnetization processes in 2 μm × 2 μm × 0.04 μm permalloy particles. *J. Appl. Phys.* **1996**, *79*, 5075.
(5) Jubert, P.-O.; Toussaint, J.-C.; Fruchart, O.; Meyer, C.; Samson, Y. Flux-closure-domain states and demagnetizing energy determination in sub-micron size magnetic dots. *Europhys. Lett.* **2003**, *63*, 132.

© 2010 American Chemical Society

DOI: 10.1021/nl102566y | *Nano Lett.* **2010,** *10,* 4200–4205

(6) Shinjo, T.; Okuno, T.; Hassdorf, R.; Shigeto, K.; Ono, T. Magnetic Vortex Core Observation in Circular Dots of Permalloy. *Science* **2000**, *289*, 930.
(7) Wachowiak, A.; Wiebe, J.; Bode, M.; Pietzsch, O.; Morgenstern, M.; Wiesendanger, R. Direct Observation of Internal Spin Structure of Magnetic Vortex Cores. *Science* **2002**, *298*, 18.
(8) Harrison, R. J.; Dunin-Borkowski, R. E.; Putnis, A. Direct imaging of nanoscale magnetic interactions in minerals. *Proc. Natl. Acad. Sci. U.S.A.* **2002**, *99*, 16561.
(9) Choe, S.-B.; Acremann, Y.; Scholl, A.; Bauer, A.; Doran, A.; Stohr, J.; Padmore, H. A. Vortex core-driven magnetization dynamics. *Science* **2004**, *304*, 420.
(10) Zhu, F. Q.; Chern, G. W.; Tchernyshyov, O.; Zhu, X. C.; Chien, C. L. Magnetic bistability and controllable reversal of asymmetric ferromagnetic nanorings. *Phys. Rev. Lett.* **2006**, *96*, No. 027205.
(11) Roy, P. E.; Lee, J. H.; Trypiniotis, T.; Anderson, D.; Jones, G. A. C.; Tse, D.; Barnes, C. H. W. Antivortex domain walls observed in permalloy rings via magnetic force microscopy. *Phys. Rev. B* **2009**, *79*, No. 060407.
(12) Naumov, I. I.; Bellaiche, L.; Fu, H. Unusual phase transitions in ferroelectric nanodisks and nanorods. *Nature* **2004**, *432*, 737.
(13) Fu, H.; Bellaiche, L. Ferroelectricity in barium titanate quantum dots and wires. *Phys. Rev. Lett.* **2003**, *91*, 257601.
(14) Kornev, I.; Fu, H.; Bellaiche, L. Ultrathin films of ferroelectric solid solutions under a residual depolarizing field. *Phys. Rev. Lett.* **2004**, *93*, 196104.
(15) Ponomareva, I.; Naumov, I.; Bellaiche, L. Low-dimensional ferroelectrics under different electrical and mechanical boundary conditions: Atomistic simulations. *Phys. Rev. B.* **2005**, *72*, 214118.
(16) Prosandeev, S.; Ponomareva, I.; Kornev, I.; Naumov, I.; Bellaiche, L. Controlling toroidal moment by means of an inhomogeneous static field: An ab initio study. *Phys. Rev. Lett.* **2006**, *96*, 237601.
(17) Gruverman, A.; Wu, D.; Fan, H.-J.; Vrejoiu, I.; Alexe, M.; Harrison, R. J.; Scott, J. F. Vortex ferroelectric domains. *J. Phys.: Condens. Matter.* **2008**, *20*, 342201.
(18) Dawber, M.; Jung, D. J.; Scott, J. F. Perimeter effect in very small ferroelectrics. *Appl. Phys. Lett.* **2003**, *82*, 436.
(19) Rodriguez, B. J.; Gao, X. S.; Liu, L. F.; Lee, W.; Naumov, I. I.; Bratkovsky, A. M.; Hesse, D.; Alexe, M. Vortex polarization states in nanoscale ferroelectric arrays. *Nano Lett.* **2009**, *9*, 1127.
(20) Schilling, A.; Byrne, D.; Catalan, G.; Weber, K.; Genenko, Y.; Wu, G.; Scott, J. F.; Gregg, J. M. Domains in Ferroelectric Nanodots. *Nano Lett.* **2009**, *9*, 3359.
(21) Ivry, Y.; Chu, D. P.; Scott, J. F.; Durkan, C. Flux Closure Vortexlike Domain Structures in Ferroelectric Thin Films. *Phys. Rev. Lett.* **2010**, *104*, 207602.
(22) Balke, N.; Choudhury, S.; Jesse, S.; Huijben, M.; Chu, Y. H.; Baddorf, A. P.; Chen, L. Q.; Ramesh, R.; Kalinin, S. V. Deterministic control of ferroelastic switching in multiferroic materials. *Nat. Nanotechnol.* **2009**, *4*, 868.
(23) Schilling, A.; Adams, T.; Bowman, R. M.; Gregg, J. M. Strategies for gallium removal after focused ion beam patterning of ferroelectric oxide nanostructures. *Nanotechnology* **2007**, *18*, No. 035301.
(24) Kalinin, S. V.; Rodriguez, B. J.; Jesse, S.; Shin, J.; Baddorf, A. P.; Gupta, P.; Jain, H.; Williams, D. B.; Gruverman, A. Vector Piezoresponse Force Microscopy. *Microsc. Microanal.* **2006**, *12*, 206.
(25) Nath, R.; Hong, S.; Klug, J. A.; Imre, A.; Bedzyk, M. J.; Katiyar, R. S.; Auciello, O. Effects of cantilever buckling on vector piezoresponse force microscopy imaging of ferroelectric domains in $BiFeO_3$ nanostructures. *Appl. Phys. Lett.* **2010**, *96*, 163101.
(26) McGilly, L.; Byrne, D.; Harnagea, C.; Schilling, A.; Gregg, J. M. Imaging domains in $BaTiO_3$ single crystal nanostructures: comparing information from transmission electron microscopy and piezo-force microscopy. *J. Mater. Sci.* **2009**, *44*, 5197.
(27) Schilling, A.; Bowman, R. M.; Catalan, G.; Scott, J. F.; Gregg, J. M. Morphological Control of Polar Orientation in Single-Crystal Ferroelectric Nanowires. *Nano Lett.* **2007**, *7*, 3787.
(28) Arlt, G.; Sasko, P. Domain configuration and equilibrium size of domains in $BaTiO_3$ ceramics. *J. Appl. Phys.* **1980**, *51*, 4956.
(29) Srolovitz, D. J.; Scott, J. F. Clock-model description of incommensurate ferroelectric film and of nematic-liquid-crystal films. *Phys. Rev. B* **1986**, *34*, 1815.

© 2010 American Chemical Society

DOI: 10.1021/nl102566y | *Nano Lett.* **2010,** *10,* 4200–4205